Thermal Runaway of Conduction-Cooled Monofilament and Multifilament Coated Conductors

Xijie Luo, Yifan Zhao, Yusuke Sogabe, *Member, IEEE*, Hisaki Sakamoto, Satoshi Yamano, Naoyuki Amemiya, *Senior Member, IEEE*

***Abstract*—We experimentally studied the thermal runaway initiating at a low critical current (I_c) part. This low I_c part is determined by the combination of two reasons in a real coil: (a) the unavoidable defects caused by the manufacturing process, which reduce local critical currents (and might not be uniform across the width of a coated conductor) and (b) the magnetic field distribution along the coated conductor. To simulate the thermal runaway using a short monofilament/multifilament $REBa_2Cu_3O_y$ (RE-123) coated conductor, we artificially created a local defect (low I_c part) in a short sample by pressing using a drill bit (creating a defect close to one edge of a coated conductor) or bending (creating a uniform defect across the width of a coated conductor). The sample of the coated conductor was conduction-cooled to 30 K, and a magnetic field was applied ($\mu_0 H$ up to 2 T) perpendicular to the wide face of the conductor to control its critical current. Transverse voltages in a multifilament coated conductor were measured to obtain the transverse currents among the filaments through the copper layer. Thermal runaway currents (operating currents above which thermal runaway initiates) of the monofilament sample and those of the multifilament sample with additional Joule loss due to the transverse currents were determined and compared to study the effect of the transverse currents on the initiation of thermal runaway in the multifilament coated conductor. Experiments on the protection against thermal runaway were conducted. When a normal voltage (over a preset threshold) was detected, the supplied current would be decreased exponentially. The thresholds for protecting monofilament and multifilament coated conductors from degradation after thermal runaway were compared.**

***Index Terms*— Coated conductor, conduction cooling, quench protection, thermal runaway.**

I. Introduction

INTRINSICALLY, local defects reduce local critical currents and are not avoidable in a coated conductor even by using the most advanced manufacturing technology [1–6].

Manuscript receipt and acceptance dates will be inserted here. This work was supported in part by JST-Mirai Program Grant Number JPMJMI19E1, JSPS KAKENHI Grant Number JP16H02326, and Japan-U.S. Science and Technology Cooperation Program in High Energy Physics. *(Corresponding author: Naoyuki Amemiya)*

X. Luo, Y. Zhao, Y. Sogabe, and N. Amemiya are with the Department of Electrical Engineering, Kyoto University, Kyoto 615-8510, Japan (e-mail: amemiya.naoyuki.6a@kyoto-u.ac.jp).

H. Sakamoto is with HTS Engineering Department, Furukawa Electric Co., Ltd, 2-6-4, Otemachi, Chiyodaku, Tokyo 100-8322, Japan.

S. Yamano is with SuperPower Inc., 21 Airport Road, Glenville, NY 12302 USA.

Color versions of one or more of the figures in this paper are available online at http://ieeexplore.ieee.org.

Digital Object Identifier will be inserted here upon acceptance.

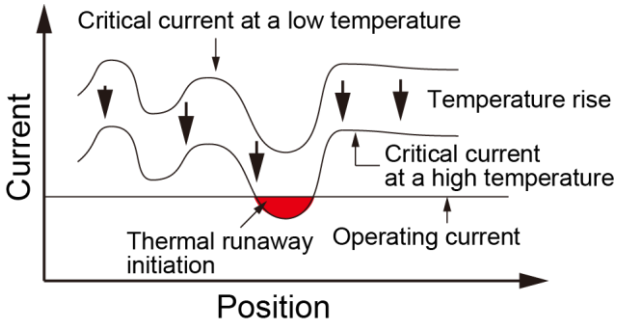

Fig. 1. Possible distribution of critical current along a conductor in a real coil and initiation of thermal runaway.

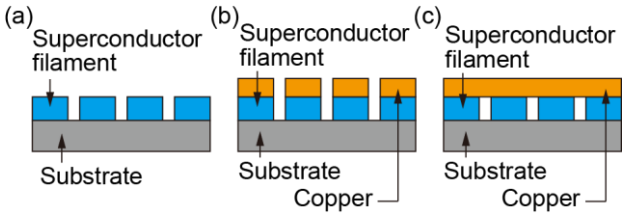

Fig. 2. Cross sections of three variations of multifilament coated conductors. (a) Without copper layer. (b) With copper layer on each filament. (c) With copper layer on the entire group of filaments.

Additionally, because the magnitude and direction of the magnetic field vary along the length of a coated conductor in a coil, its critical current, which depends on these parameters, also varies [7, 8], and the local critical current is suppressed by the magnetic field at some parts of the conductor (I_c suppression by magnetic field). Owing to local defects and I_c suppression by the magnetic field, the critical current along a conductor in a real coil can be distributed, as shown in Fig. 1, and low I_c parts appear. When there is an unexpected temperature rise of the coil, caused by the cooling system or heating by radiation in the case of accelerator or fusion magnets, etc., the critical current decreases and thermal runaway might initiate at the weakest point, at which the local critical current I_c is lower than in other parts of the coil, as shown in Fig. 1.

To reduce ac losses and shielding current-induced fields in a coated conductor [9–12], three variations of multifilament coated conductors have been proposed, as shown in Fig. 2: (a) multifilament coated conductor without copper layer; (b) multifilament coated conductor with copper layer on each filament; (c) multifilament coated conductor with copper layer on the entire group of filaments. When there are local defects in the multifilament coated conductors, the current in the filaments with defects is blocked in the coated conductors, as

shown in Figs. 2(a) and (b); the current can bypass the defects through the copper layer and sound filaments in the coated conductor, as shown in Fig. 2(c). In this study, we focused on the thermal runaway of multifilament coated conductor shown in Fig. 2(c), which is preferable from the viewpoint of current sharing among filaments. However, the Joule loss generated in the copper layer by bypassing the current is a concern when compared with monofilament coated conductor, as it may initiate thermal runaway and affect protection after detecting thermal runaway.

Numerical and experimental studies have been conducted on the initiation of thermal runaway in monofilament coated conductors [13–21]. However, the initiation of thermal runaway in multifilament coated conductors has not been experimentally studied. Furthermore, previous experimental studies on thermal runaway did not directly discuss the conditions under which the conventional quench detection and protection scheme (*i.e.*, detecting quench/thermal runaway using voltage taps and dumping the stored energy in an external dump resistor) could be applied [22–32].

The objective of this study is to clarify and compare the behaviors (voltage, current, temperature, etc.) of monofilament and multifilament coated conductors during the following process:

1) initiation process of thermal runaway;
2) detection and protection process against thermal runaway.

In the initiation process of thermal runaway, the voltages/currents (in the longitudinal and transverse directions) and thermal runaway currents on the monofilament and multifilament were measured and compared. In the detection and protection process against thermal runaway, as a threshold for protecting coated conductors from degradation, the *protectable currents* (below which the conductor can be protected) of monofilament and multifilament coated conductors were determined and compared.

II. Coated Conductors Used in Experiments and Experimental Method

A. Coated Conductors Used in Experiments

The monofilament coated conductors used in this study were the standard copper-plated coated conductors SCS4050 of SuperPower Inc. The multifilament coated conductors we used were developed by Furukawa Electric Co., Ltd. and SuperPower Inc. based on the SCS4050: the superconductor layer was divided into five filaments by laser striation and subsequently plated with copper (thickness: 20 μm) [9, 10]. The detailed specifications of the monofilament and multifilament coated conductors are listed in Table I.

The thermal runaway behaviors (voltage, current, temperature, etc.) of multifilament coated conductors with a copper layer on the entire group of filaments (shown in Fig. 2(c)) might be different from those of monofilament coated conductors. In a monofilament coated conductor, when there is a local defect close to one edge, as shown in Fig. 3(a), the current

TABLE I
SPECIFICATIONS OF SAMPLES

Properties	SCS4050 (Monofilament)	SCS4050 (Multifilament)
Manufacturer	SuperPower	Furukawa/SuperPower
Number of filaments	1	5
Width	4 mm	4 mm
Entire thickness	0.1 mm	0.1 mm
Plated-copper thickness	20 μm	20 μm
Thickness of silver protective layer	~3.8 μm	~3.8 μm
Thickness of Hastelloy substrate	50 μm	50 μm
Critical current (temperature, magnetic field)	~ 240 A (30 K, 2 T)	~ 240 A (30 K, 2 T)

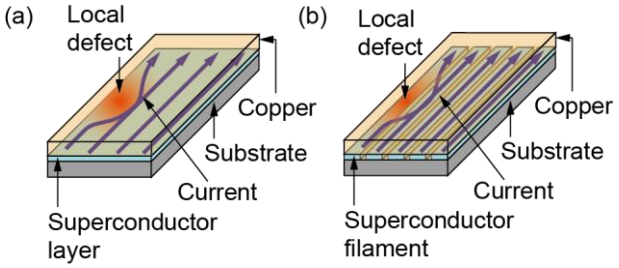

Fig. 3. Current distribution in the coated conductor with local defect. (a) Monofilament coated conductor. (b) Multifilament coated conductor.

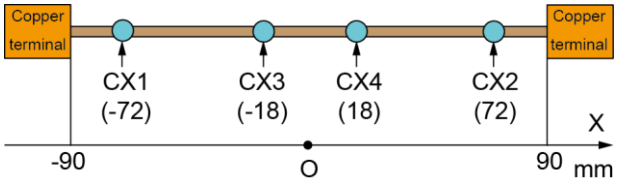

Fig. 4. Sample layout and positions of temperature sensors (CX*i*: Cernox temperature sensor). Numbers in blankets are relative positions to the longitudinal center of the short sample (unit: millimeter).

can bypass the local defect within its superconductor layer. In this case, there is no Joule loss because the current flows in the superconductor layer only. However, in the multifilament coated conductor with a copper layer on the entire group of filaments (shown in Fig. 2(c)), if there is a local defect in a filament close to one edge, as shown in Fig. 3(b), the current might bypass the local defect through the copper layer and sound filaments on the other side. The transverse part of the bypass current, which flows through the copper layer, might generate an additional Joule loss and subsequently initiate thermal runaway.

B. Experimental Method

In this section, we explain the experimental method that is common for the experiments of III and IV.

Instead of using expensive coils, we conducted experiments using short samples of monofilament and multifilament coated conductors, whose effective lengths between the copper terminals injecting current were 180 mm, as shown in Fig. 4. The sample was conduction-cooled by a cryocooler, and its temperature was PID-controlled at 30 K using the temperature measured by temperature sensors CX1 and CX2 shown in Fig. 4, as well as heaters (not shown in Fig. 4) near the copper

terminals in all experiments. The side closer to superconductor layer of the tape-shaped coated conductor faced vacuum, and the other face was attached to a glass fiber reinforced plastics (GFRP) sample holder using epoxy resin and polyimide tape. In this study, all of the voltage taps were attached on the side closer to the superconductor layer. A magnetic field perpendicular to the wide face of the sample was applied to control the critical current.

To simulate thermal runaway initiating at the weakest point (the I_c is lower than other parts) in a real coil shown in Fig. 1 using a short sample, we artificially created a local defect at the longitudinal center of the short sample. The details are explained in Sections III and IV.

We initiated a thermal runaway by increasing the current stepwise: we increased the current, maintained the current constant for a certain time (holding time, 300 s or 30 min in this study) to verify whether it was thermally running away or not, and if not, we increased the current again. This procedure was repeated until thermal runaway was detected. Here, we considered that a sample thermally ran away if the voltage across the entire sample exceeded 20 mV. Herein, we discuss the thermal runaway current by using *300 s-thermal runaway current* or *30 min-thermal runaway current*, which is defined as the current at which thermal runaway initiates in 300 s or 30 min after the current reaches this value.

III. Initiation of Thermal Runaway of Monofilament and Multifilament Coated Conductors

A. Purpose of Experiments

In a multifilament coated conductor, the manufacturing process may cause local defects in certain filaments. We focused on the multifilament coated conductor with copper layer on the entire group of filaments (Fig. 2(c)), in which the current can bypass the local defects through the copper layer and sound filaments. When compared with a monofilament coated conductor, the Joule loss generated in the copper layer by bypassing current (transverse current through the copper layer) is a concern, which might affect the initiation of thermal runaway.

The purpose of this part of experiments is:

1) to confirm current bypassing through the copper layer to prevent current blocking by the defect;
2) to determine how an additional Joule loss by bypassing the current through the copper layer affects the initiation of thermal runaway in a multifilament coated conductor.

B. Samples and Procedure of Experiments

To create a local defect in the filament close to one edge of the sample (as shown in Fig. 3) and to initiate thermal runaway at the longitudinal center of the sample, we pressed the monofilament/multifilament samples using a drill bit near the voltage tap section a3–a4, as shown in Fig. 5 (the area of the degraded superconductor layer might be larger than the ϕ0.7 mm section shown in Fig. 5 because the superconductor layer near the pressed area might also suffer some stress). The purpose of creating a local defect was to simulate the situation in Fig. 3 (caused by the manufacturing process) and not to study the conductor with this particular damage.

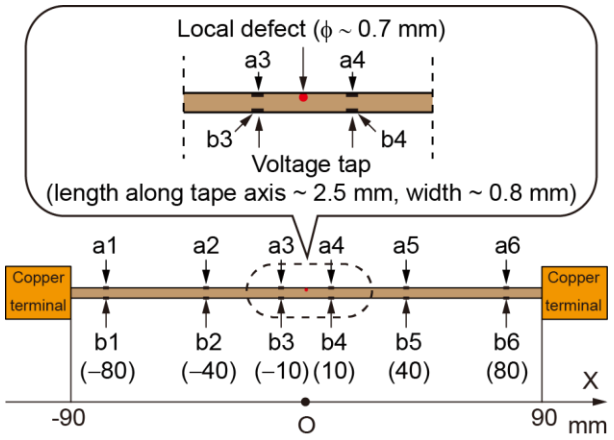

Fig. 5. Positions and geometry of voltage taps attached at the edges of the sample (a*i*/b*i*: voltage tap). Numbers in blankets are relative positions to the longitudinal center of the short sample (unit: millimeter).

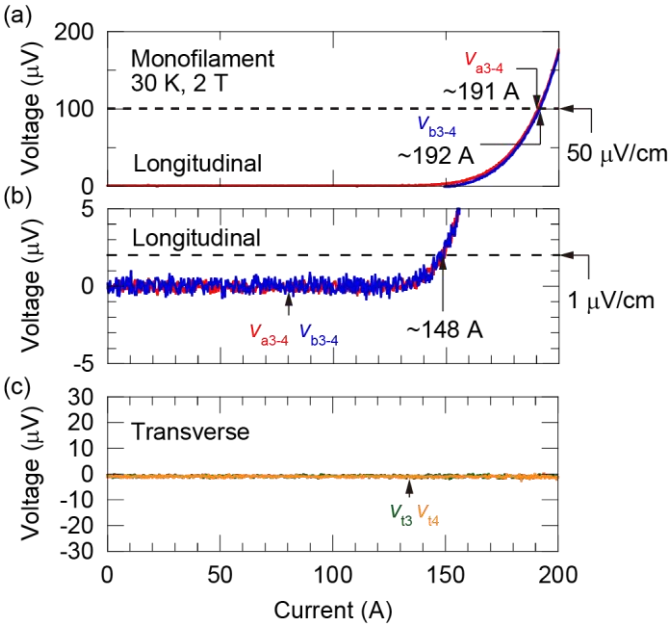

Fig. 6. Voltage–current characteristics of monofilament sample with local defect at 30 K, 2T. (a) Voltages on longitudinal direction. (b) Voltages on longitudinal direction (enlarged). (c) Voltages on transverse direction. ($v_{am\text{-}n}$: voltage between tap a*m* and a*n*; $v_{bm\text{-}n}$: voltage between tap b*m* and b*n*; v_{ti}: voltage between tap a*i* and b*i*).

The positions of the voltage taps of the monofilament/multifilament samples in this part of the experiments are shown in Fig. 5. Voltage taps were attached at the edges of the sample (voltage taps from a1 to a6 on one side and from b1 to b6 on the opposite side) to measure the longitudinal voltages $v_{am\text{-}n}$, $v_{bm\text{-}n}$ (voltages between the taps a*m* and a*n*, b*m* and b*n*, respectively) and transverse voltages v_{ti} (voltages between the taps a*i* and b*i*). Each voltage tap's length along tape axis was ~2.5 mm, and its width was ~0.8 mm, respectively. In principle, an instrument for voltage measurements detects the potential (voltage) at the location where the fine signal wire from the instrument is attached. Note that the small wire cross section as well as the high input impedance of the instrument is

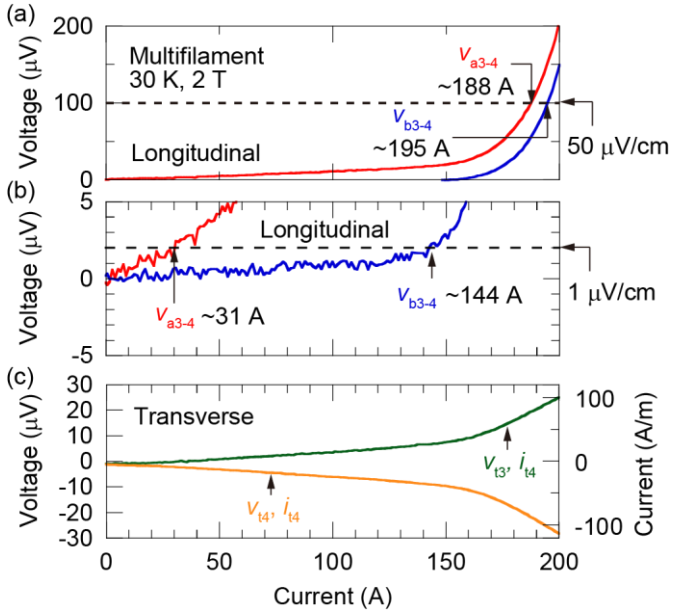

Fig. 7. Voltage–current characteristics of multifilament sample with local defect at 30 K, 2T. (a) Voltages on longitudinal direction. (b) Voltages on longitudinal direction (enlarged). (c) Voltages/currents on transverse direction. ($v_{am\text{-}n}$: voltage between tap a*m* and a*n*; $v_{bm\text{-}n}$: voltage between tap b*m* and b*n*; v_{ti}/i_{ti}: voltage/current between tap a*i* and b*i*).

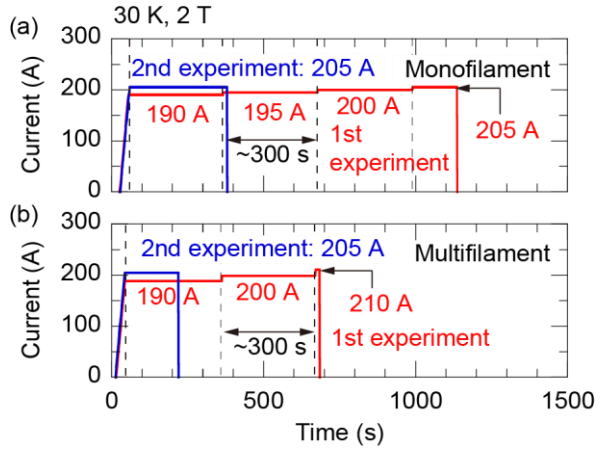

Fig. 8. Processes to determine *300 s-thermal runaway currents*. (a) Monofilament sample; (b) Multifilament sample.

important, because the entire volume of the signal wire must be equipotential. If the signal wire is attached to a large solder spot or a large metal tip (if any) on a sample, the instrument measures the potential (voltage) at the location on the solder spot or the metal tip where the signal wire is attached, rather than that of the sample. In this case, the measured voltage might be affected by the voltage drop caused by the current flowing inside the solder spot or the metal tip. Therefore, smaller solder spot (without any metal tip) is better for more precise measurement. From the transverse voltages and the transverse conductance between filaments, we calculated the transverse current in multifilament coated conductors. The process to obtain the transverse conductance is described in Appendix.

All the experiments in III were conducted at 30 K, 2 T. Fig. 6 illustrates the voltage–current (*V–I*) characteristics of a monofilament sample with local defects. As shown in

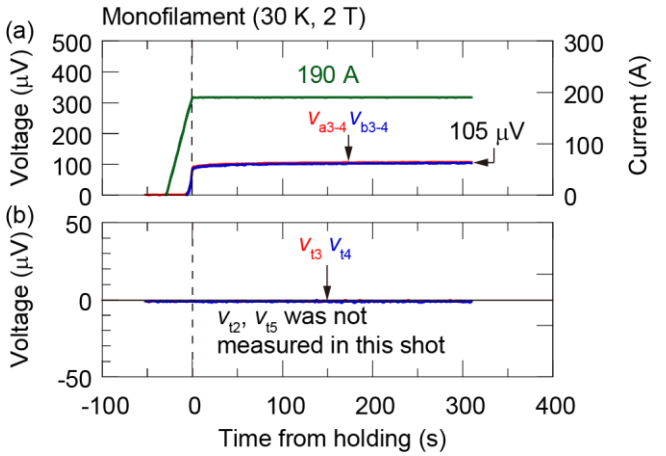

Fig. 9. Example of voltages and current of monofilament sample with local defect at 190 A, 30 K, 2 T (no thermal runaway initiates in 300 s). (a) Voltages on longitudinal direction. (b) Voltages on transverse direction. (after the current reached 190 A in Fig. 8(a), 1st experiment; vam-n: voltage between tap am and an; vbm-n: voltage between tap bm and bn; vti: voltage between tap ai and bi).

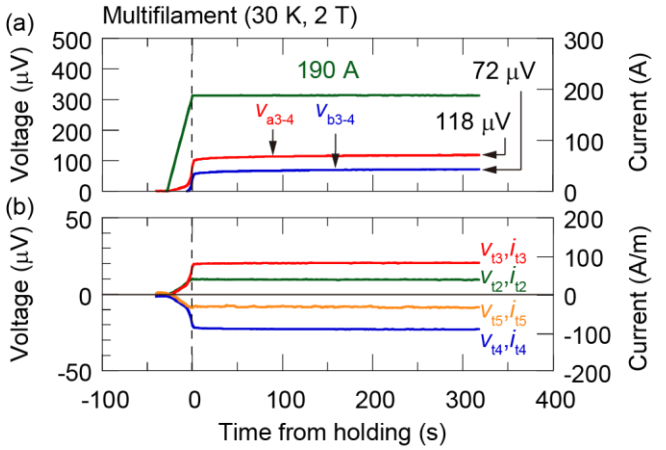

Fig. 10. Example of voltages and currents of multifilament sample with local defect at 190 A, 30 K, 2 T (no thermal runaway initiated in 300 s). (a) Voltages on longitudinal direction. (b) Voltages and currents on transverse direction (after the current reached 190 A in Fig. 8(b), 1st experiment; $v_{am\text{-}n}$: voltage between tap a*m* and a*n*; $v_{bm\text{-}n}$: voltage between tap b*m* and b*n*; v_{ti}/i_{ti}: voltage/current between tap a*i* and b*i*).

Figs. 6(a) and (b), the longitudinal voltages $v_{a3\text{-}4}$ and $v_{b3\text{-}4}$, on the opposite side, were almost the same. As shown in Fig. 6(c), the transverse voltages v_{t3} and v_{t4} were nearly zero, which suggests that no current flowed in the copper layer in the transverse direction in the monofilament sample.

The *V–I* characteristics of the multifilament sample with local defects are shown in Fig. 7. As shown in Figs. 7(a) and (b), the longitudinal voltage $v_{a3\text{-}4}$ between taps a3 and a4, which were close to the local defect, was higher than the longitudinal voltage $v_{b3\text{-}4}$ on the opposite side. In other words, the conductor was not equipotential laterally. The voltages in the transverse direction v_{t3} and v_{t4} shown in Fig. 7(c) suggest that transverse currents flowed in the a3→b3 and b4→a4 directions through the copper layer. The sample currents at which the electric fields between a3–a4 and b3–b4 reached 1 μV/cm, which is the standard criterion to define critical current, were 31 A and 144 A, respectively. Because the concept of critical current implicitly assumes that a conductor is equipotential in

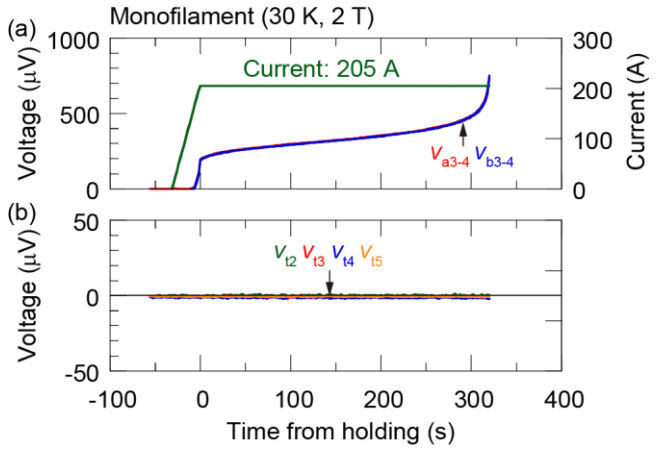

Fig. 11. Example of voltages and current of monofilament sample with local defect at 205 A, 30 K, 2 T (thermal runaway initiated). (a) Voltages on longitudinal direction. (b) Voltages on transverse direction (one shot of the repeated experiments of Fig. 8(a), 2nd experiment; $v_{am\text{-}n}$: voltage between tap a*m* and a*n*; $v_{bm\text{-}n}$: voltage between tap b*m* and b*n*; v_{ti}: voltage between tap a*i* and b*i*).

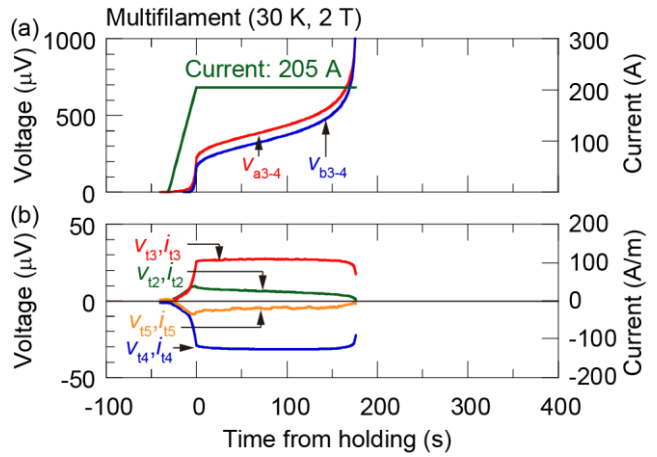

Fig. 12. Example of voltages and currents of multifilament sample with local defect at 205 A, 30 K, 2 T (thermal runaway initiated). (a) Voltages on longitudinal direction. (b) Voltages/currents on transverse direction (after the current reached 205 A in Fig. 8(b), 2nd experiment; $v_{am\text{-}n}$: voltage between tap a*m* and a*n*; $v_{bm\text{-}n}$: voltage between tap b*m* and b*n*; v_{ti}/i_{ti}: voltage/current between tap a*i* and b*i*).

its lateral cross section, we might be not able to define a unique critical current in this case. As a reference, currents reaching a higher electric field of 50 μV/cm, for example, are less dependent on the arrangements of voltage taps (188 A and 195 A, respectively), because the large electric field appeared in the entire cross section of the conductor, and the contribution of the transverse voltage became negligible. The right axis of Fig. 7(c) is the scale of the transverse current in the unit length along the coated conductor calculated from v_{t3}, v_{t4}, and the transverse conductance 4.03×10^9 S/m across four striations between filaments (see Appendix).

To clarify how the additional Joule loss (generated by the transverse current through the copper layer) affects the initiation of thermal runaway in a multifilament coated conductor, we compared the *300 s-thermal runaway current* of a multifilament coated conductor with that of a monofilament coated conductor. Notice that the local defect was created close to the edge of each sample. The process to determine the *300 s-thermal runaway current* values is shown as the first experiment in Fig. 8. After determining these values, the second experiment shown in Fig. 8 was conducted at the determined *300 s-thermal runaway current* (or a slightly lower current) repeatedly, to examine the thermal runaway process in detail. The thermal runaway current might be different in a real coil, depending on the cooling condition.

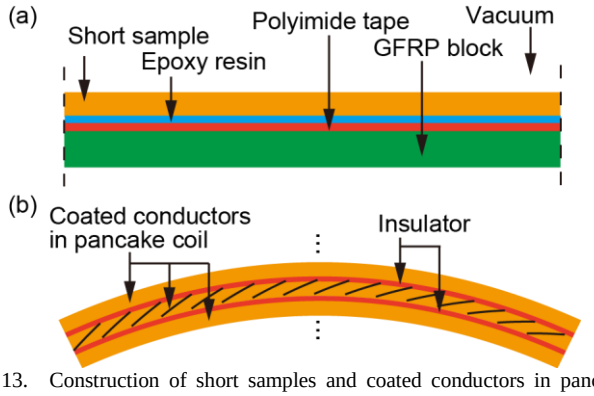

Fig. 13. Construction of short samples and coated conductors in pancake coil across their thicknesses. (a) Short sample. (b) Coated conductors in middle turns of pancake coil.

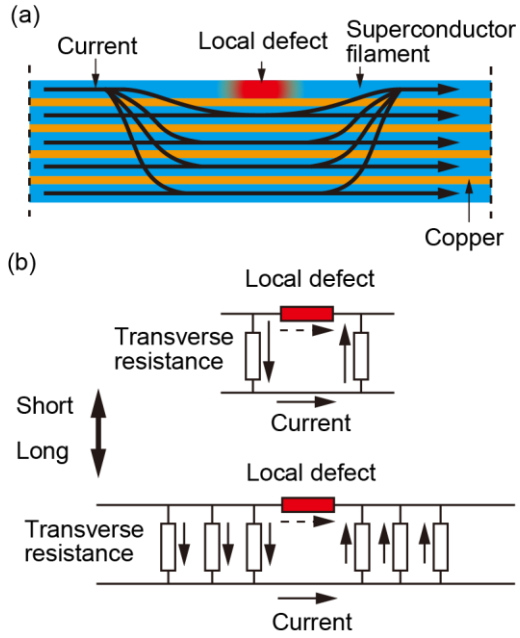

Fig. 14. Possible current distribution in a multifilament coated conductor with local defect. (a) Current distribution among superconductor filaments. (b) Equivalent circuit.

C. *Experimental Results*

Examples of voltages/currents of monofilament/multifilament samples when no thermal runaway was detected in 300 s (after the current reached 190 A in Fig. 8, 1st experiment) are shown in Figs. 9 and 10, respectively. In both the monofilament and multifilament samples, the longitudinal voltages $v_{a3\text{-}4}$ and $v_{b3\text{-}4}$ (shown in Figs. 9(a) and 10(a), respectively) were nearly stable after the current reached 190 A, which suggests that the temperatures at the longitudinal center of these two samples were stable. As shown in Fig. 10(b), transverse voltages/currents (several tens of A/m) were ob-

served in the multifilament sample. In this case, the additional Joule loss generated by the transverse current through the copper layer could be removed by the cryocooler, and thermal runaway was not initiated in the multifilament sample.

Examples of voltages/currents of monofilament/multifilament samples when thermal runaway was detected (operating current: 205 A) are shown in Figs. 11 and 12, respectively. In the monofilament (Fig. 11) and multifilament (Fig. 12) samples, thermal runaway initiated approximately 300 s and 200 s after the current reached 205 A, respectively. The transverse voltages/currents (v_{t2}/i_{t2}, v_{t3}/i_{t3}, v_{t4}/i_{t4}, v_{t5}/i_{t5}) shown in Fig. 12(b) suggest that before thermal runaway was detected, the transverse current flowed through the copper layer (several tens of A/m) in the multifilament sample. An additional Joule loss generated by this transverse current might have caused earlier initiation of thermal runaway in multifilament coated conductor.

The initiation of thermal runaways in the short samples might be different from those in real coils. The cooling conditions of the conductors in short samples and those in real coils may be different; for example, as shown in Fig. 13: (a) in a short sample, because one side of the tape shape conductor faces a vacuum, the conductor is mainly cooled from another side through epoxy resin, polyimide tape, and GFRP sample holder; (b) in an insulated pancake coil, for example, the tape shape conductor in middle turns could be cooled from two sides through insulators and other turns of conductors. In real coils wound by multifilament coated conductors, the Joule loss generated by the transverse current among filaments might be different from that in short samples. The possible current distribution in a multifilament coated conductor with a local defect is shown in Fig. 14. In real coils, because the conductors are considerably longer than those in short samples, the bypassing current diffuses in longer parts along the conductor, as shown in Fig. 14(b), and the transverse current density is smaller than that in short samples. Because the transverse resistance is lower in a longer conductor, when bypassing the same amount of current, the total Joule loss in real coils is smaller than that in short samples. Compared with short samples, because both the localized Joule loss (determined by transverse current density) and total Joule loss should be smaller, the bypassing current does not significantly affect the thermal runaway current in real coils.

IV. Thermal Runaway Detection and Protection of Monofilament and Multifilament Coated Conductors

A. Purpose of Experiments

The conventional quench/thermal runaway detection and protection process is widely used in superconducting coils: the voltage across a superconducting coil is monitored by voltage taps; if it exceeds a voltage threshold (detection voltage), a circuit breaker is activated; subsequently, the coil current is transferred to the external dump resistor and decays exponentially with a time constant equal to the coil inductance/resistance of the dump resistor [25].

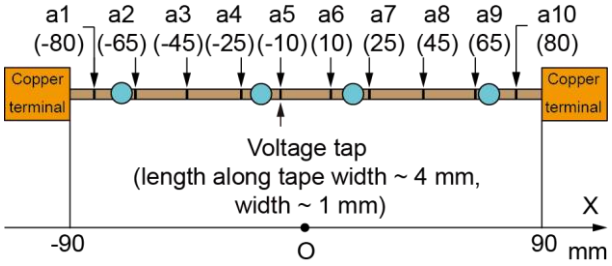

Fig. 15. Positions and geometry of voltage taps of monofilament sample in thermal runaway detection and protection experiments (*ai*: voltage tap). Numbers in blankets are relative positions to the longitudinal center of the short sample (unit: millimeter).

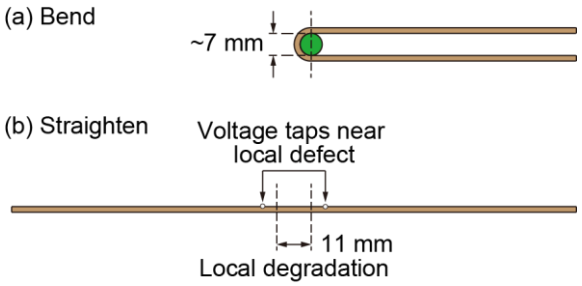

Fig. 16. Side view of sample with local defect (by bending). (a) Bending sample to create a local and uniform defect across its width (~11 mm length). (b) Straightened sample.

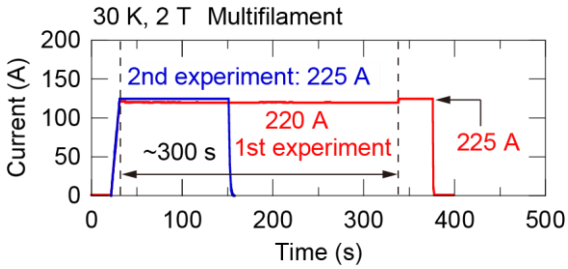

Fig. 17. Example of processes to determine the *300 s-thermal runaway currents* in multifilament sample in thermal runaway detection and protection experiments (30 K, 2 T).

In a real coil, the initiation of the thermal runaway is determined by whether the power of Joule loss is larger than the cooling power. Under certain cooling conditions, because the amount of Joule loss is determined by the amount of current flowing in the copper layer (operating current – critical current, based on the current sharing model), the thermal runaway current is determined by the critical current, which depends on the temperature and magnetic field distribution in a real coil. In this part of the experiments, we studied the detection and protection process against thermal runaway at various thermal runaway currents, which are influenced by critical currents.

The purpose of this part of the experiments is to determine whether there are significant differences in the threshold for protecting monofilament and multifilament coated conductors from degradation by comparing the hot-spot temperature and *protectable current* between these conductors, using the conventional detection and protection method.

B. Samples and Procedure of Experiments

The positions and geometry of the voltage taps of the monofilament samples in this part of the experiments are shown in Fig. 15, whereas those of the multifilament were the same as

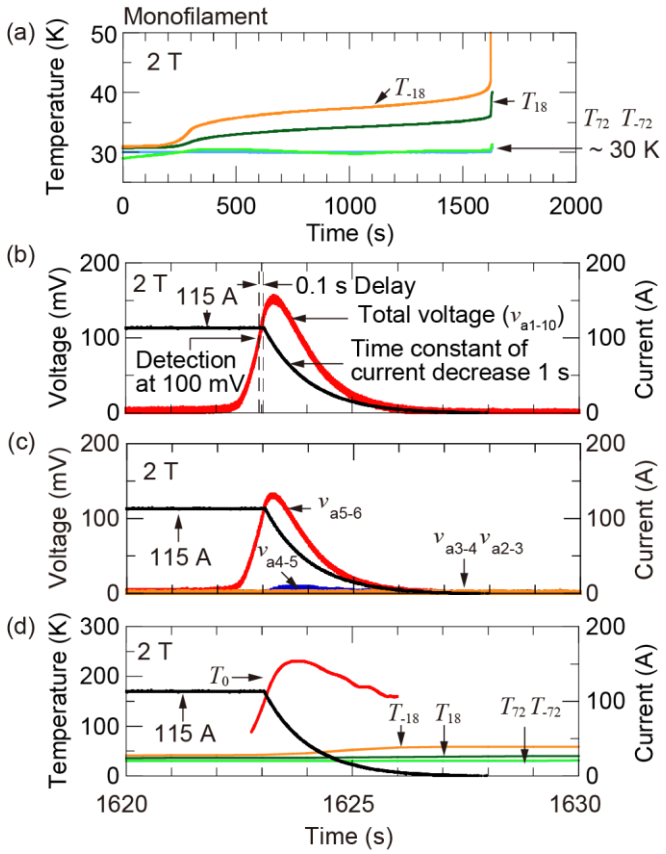

Fig. 18. Example of voltages/currents/temperatures of thermal runaway detection and protection processes (monofilament sample) at 2 T, 115 A.f (a) Temperatures when the current started flowing to thermal runaway. (b) Total voltage when thermal runaway initiated. (c) Voltages on plus side when thermal runaway initiated. (d) Temperatures when thermal runaway initiated. ($v_{am\text{-}n}$: voltage between tap a*m* and a*n*; $v_{bm\text{-}n}$: voltage between tap b*m* and b*n*; v_{ti}: voltage between tap a*i* and b*i*; T_x: temperature at position *x*).

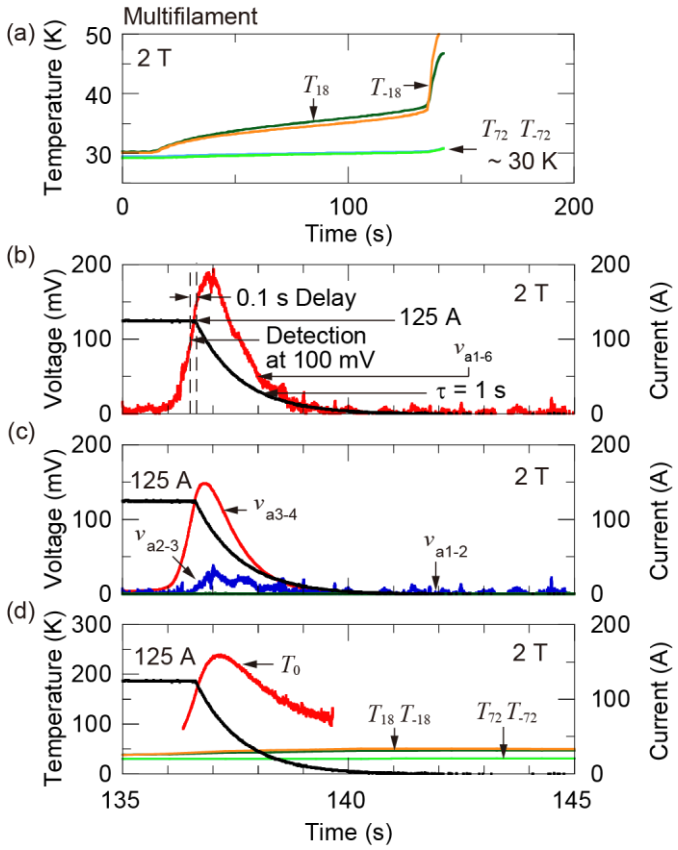

Fig. 19. Example of voltages/currents/temperatures of thermal runaway detection and protection process (multifilament sample) at 2 T, 125 A. (a) Temperatures when the current started flowing to thermal runaway. (b) Total voltage when thermal runaway initiated. (c) Voltages on plus side when thermal runaway initiated. (d) Temperatures when thermal runaway initiated. ($v_{am\text{-}n}$: voltage between tap a*m* and a*n*; $v_{bm\text{-}n}$: voltage between tap b*m* and b*n*; v_{ti}: voltage between tap a*i* and b*i*; T_x: temperature at position *x*).

those shown in Fig. 3. In monofilament samples (Fig. 15), each voltage tap's length along tape width was ~4 mm, and its width was ~1 mm, respectively. To locate the place at which thermal runaway initiates and easily control the *300 s-thermal runaway current*, we created a local and uniform defect across the width of a coated conductor by bending the samples using a rod, as shown in Fig. 16. It should be noted that all of the defects were created by bending (to control the critical current easily) instead of pressing using a drill bit (Fig. 5) in the sample described in this section. From the viewpoint of thermal runaway detection and protection, there should be no difference between the samples with different types of defects, because most of the current flows in the copper layer after thermal runaway.

Thermal runaway currents were determined using the method introduced in Section II. *B*. The holding times were different in the experiments using monofilament conductors (~30 min) and those multifilament conductors (300 s). Although this difference influences the thermal runaway currents, they were controlled by varying applied magnetic fields, which vary the critical currents. As shown in Fig. 17 for a multifilament sample, after a thermal runaway current was determined in the first experiment, the second experiment was conducted at the determined thermal runaway current to determine whether the conductor can be protected at this current or not. In the second experiment, a field-programmable gate array was used to monitor the voltage and control the output of

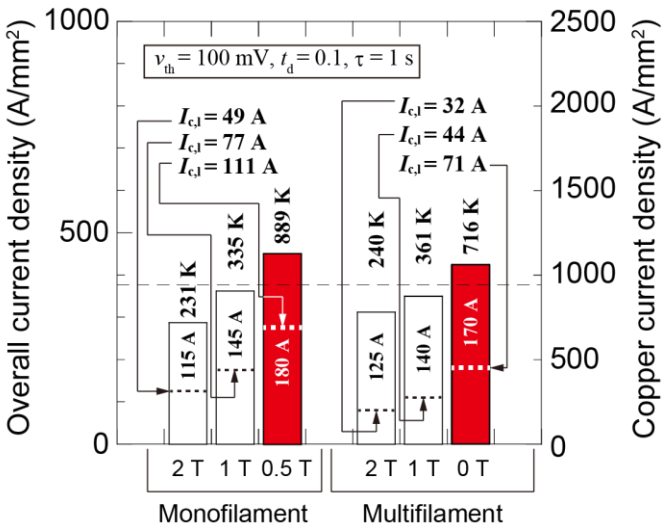

Fig. 20. Summary of the thermal runaway detection and protection experiments. White bar: after which no degradation was observed. Red bar: after which samples degraded. $I_{c,l}$: critical current at local defect measured between a5 and a6 in monofilament sample, and between a3 and a4 in multifilament sample (length: 20 mm, electric field: 100 μV/m).

TABLE II
PROTECTABLE CURRENT OF QUENCH INDUCED BY LOCAL AND TRANSIENT THERMAL DISTURBANCE

Sample	Protectable current
Monofilament	150 A
Multifilament	150 A

T_i = 30 K, B = 2 T, v_{th} = 100 mV, t_d = 100 ms, τ = 1 s

TABLE III
SUMMARY OF DETECTION AND PROTECTION AGAINST THERMAL RUNAWAYS INITIATED AT LOCAL BENDING DEFECT

Sample	I_t (T, B)	Holding time until thermal runaway	$I_{c,l}$ before and after thermal runaway	n before and after thermal runaway
Monofilament (one sample)	115 A (30 K, 2 T)	~ 30 min	before: 49 A after: 49 A	before: 16 after: 15
	145 A (30 K, 1 T)	~ 30 min	before: 77 A after: 79 A	before: 17 after: 18
	180 A (30 K, 0.5 T)	~ 10 min	before: $I_{c,l}$ = 111 A, n = 20 after: burnt out	
Multifilament (one sample)	125 A (30 K, 2 T)	~ 2 min	before: 32 A after: 32 A	before: 10 after: 9
	140 A (30 K, 1 T)	~ 4 min	before: 44 A after: 43 A	before: 8 after: 9
	170 A (30 K, 0 T)	~ 3 min	before: $I_{c,l}$ = 71 A, n = 5 after: linear V-I	

Detection and protection conditions: v_{th} = 100 mV, t_d = 0.1 s, τ = 1 s.
$I_{c,l}$: critical current at local defect measured between a5 and a6 in monofilament sample, and between a3 and a4 in multifilament sample (length: 20 mm, electric field: 100 μV/m).

the power supply [25]. Once the monitored voltage across the entire sample ($v_{a1\text{-}10}$ in monofilament sample, $v_{a1\text{-}6}$ in multifilament sample) reached a detection voltage (v_{th} = 100 mV, simulating thermal runaway / quench detection), after a period of delay (t_d = 100 ms, simulating the time required for detection in a real coil and for activating the circuit breaker), the sample current decreased exponentially (τ = 1 s, simulating current decay by the dump resistor while neglecting the normal resistance of the coated conductor). The critical currents and n values before and after thermal runaway were compared to determine whether the sample was successfully protected.

We calculated the hot-spot temperature during the detection and protection process against quench/thermal runaway from the voltage at the center of the sample ($v_{a5\text{-}6}$ in monofilament sample, $v_{a3\text{-}4}$ in multifilament sample, assuming RRR = 50) based on the current sharing model and the temperature dependence of resistivity of the plated copper, which we introduced in a previous study [25].

C. Experimental Results

Examples of the voltages/currents/temperatures of the thermal runaway detection and protection process of monofilament/multifilament samples are shown in Figs. 18 and 19, respectively. The total voltages across the entire sample (used for detection) and operating currents (decreased exponentially when thermal runaway was detected) are shown in Figs. 18(b) and 19(b), respectively. In this section, the experiments were conducted using the same detection and protection conditions (v_{th} = 100 mV, t_d = 100 ms, τ = 1 s), which are reasonable for real magnets [25]. In these two experiments, the maximum temperatures in the monofilament/multifilament samples were nearly 250 K, as shown in Figs. 18(d) and Fig. 19(d). After these experiments, degradation of the critical currents and n values was not observed for both conductors.

We varied the magnetic field to vary the critical current and then varied the thermal runaway current. The results of thermal runaway detection and protection experiments conducted at various thermal runaway currents are summarized in Fig. 20. In this figure, white bars represent thermal runaway after which no degradation on critical current/n value was observed, and red bars represent thermal runaway after which samples degraded. In other words, currents of white bars are under the *protectable current*, below which the used conditions (v_{th} = 100 mV, t_d = 0.1 s, τ = 1 s) can protect coated conductors. These experimental results suggest that the *protectable currents* of monofilament/multifilament samples against thermal runaway were approximately 150 A. In this figure, the critical currents and the maximum hot-spot temperatures are also shown.

In a previous study [25], we evaluated the *protectable current* of a monofilament coated conductor (attached on the same sample holder in this study) against the quench induced by local and transient thermal disturbance (using a quench heater). Similar experiments were conducted using a multifilament coated conductor. The *protectable currents* of monofilament and multifilament samples against quench induced by local and transient thermal disturbance were 150 A, as listed in TABLE II, which is a value close to those against thermal runaway summarized in Fig. 20. This suggests that the *protectable current* does not depend on the cause of the quench/thermal runaway and the origin of degradation might be the maximum hot-spot temperature reached locally. The details of the thermal runaway experiments (holding time, critical current before and after thermal runaway, etc.) are listed in Table III.

V. CONCLUSION

We experimentally studied the thermal runaways of copper-plated multifilament and monofilament coated conductors, which were conduction-cooled by a cryocooler. In our copper-plated multifilament coated conductor, a copper layer covered the entire group of filaments and allowed current sharing among them to improve stability and to help protection. When an artificial local defect was created close to one edge of a copper-plated multifilament coated conductor, the current was successfully bypassed through copper and sound filaments on the other side. Although this bypassing current generated additional Joule loss in the copper layer, its effect on the initiation of thermal runaway was not remarkable: thermal runaway was initiated at almost the same operating current in a multifilament coated conductor as compared to a monofilament coated conductor, although it initiated earlier in the multifilament coated conductor. Once thermal runaway is initiated in a coated conductor, it is important to determine whether it can be protected. When we applied a conventional quench detection

and protection scheme, detecting by voltage and dumping energy by a resistor, that is, exponentially decreasing the current, the threshold currents for successful protection (*protectable currents*) of monofilament and multifilament coated conductors were almost at the same level.

APPENDIX

Transverse Conductance between Superconductor Filaments

We estimated the transverse conductance between superconductor filaments by comparing the experimentally determined coupling time constant of the multifilament coated conductor with that obtained from numerical analyses when varying the transverse conductance [18]. The determined transverse conductance per unit length across one striation at 77 K, $g_{s1\text{-}77K}$, was 2.7×10^9 S/m.

In this study, we conducted experiments at 30 K using a five-filament (four striations) coated conductor. Considering the resistivity–temperature relation of copper, the transverse conductance across four striations between filaments can be given as follows:

$$g_{s4\text{-}30K} = \frac{1}{4} \cdot \frac{\rho_{77K}}{\rho_{30K}} \cdot g_{s1\text{-}77K}, \tag{1}$$

where ρ_{77K} (2.27×10^{-9} Ω m) and ρ_{30K} (3.80×10^{-10} Ω m) are the resistivity of copper at 77 K and 30 K, respectively [33]. The obtained transverse conductance across four striations between filaments $g_{s4\text{-}30K}$ was 4.03×10^9 S/m.

REFERENCES

[1] L. Ren, S. Guo, G. Chen, L. Su, Y. Xu, J. Shi, and L. Chen, "Experimental research on critical current behavior of various commercial HTS tapes," *IEEE Trans. Appl. Supercond.*, vol. 30, no. 4, Jun. 2020, Art. no. 6601006.

[2] F. Gömöry, J. Šouc, M. Adámek, A. Ghabeli, M. Solovyov, and M. Vojenčiak, "Impact of critical current fluctuations on the performance of a coated conductor tape," *Supercond. Sci. Technol.*, vol. 32, Oct. 2019, Art. no. 124001.

[3] H. Ha, G. Kim, H. Noh, J. Lee, S. Moon, and S. Oh, "Fabrication of 1 m long multi layered superconducting coated conductor with high engineering critical current density," *Supercond. Sci. Technol.*, vol. 33, Feb. 2020, Art no. 044007.

[4] C. Pop, B. Villarejo, F. Pino, B. mundet, S. Ricart, M. de Palau, T. Puig, and X. Obradors, "Growth of all-chemical high critical current $YBa_2Cu_3O_{7-\delta}$ thick films and coated conductors," *Supercond. Sci. Technol.*, vol. 32, Nov. 2018, Art. no. 015004.

[5] U. Bong, J. Kim, J. Bang, J. Park, K.J. Han, and S. Hahn, "'Defect-irrelevant-winding' no-insulation (RE)$Ba_2Cu_3O_{7-x}$ pancake coil in conduction-cooling operation," *Supercond. Sci. Technol.*, vol. 34, Jun. 2021, Art. no. 085003.

[6] Y. Zhu, W. Chen, H. Zhang, L. Liu, X. Pan, X. Yang, and Y. Zhao, "Study of the inhomogeneity of critical current under in-situ tensile stress for YBCO tape," *Supercond. Sci. Technol.*, vol. 31, Feb. 2018, Art. no. 035007.

[7] Z. Yue, Z. Sun and Z. Liu, "Design and Magnetic Field Simulation of 3.0T MRI Superconducting Magnet," *IEEE Trans. Appl. Supercond.*, vol. 29, no. 2, March 2019, Art no. 4901106.

[8] E. Seiler, F. Gömöry, R. Ries, and M. Vojenčiak, "Analysis of critical current anisotropy in commercial coated conductors in terms of the maximum entropy approach," *Supercond. Sci. Technol.*, vol. 32, Jul. 2019, Art no. 095004.

[9] N. Amemiya, N. Tominaga, R. Toyomoto, T. Nishimoto, Y. Sogabe, S. Yamano, and H. Sakamoto, "Coupling time constants of striated and copper-plated coated conductors and the potential of striation to reduce shieldingcurrent-induced fields in pancake coils," *Supercond. Sci. Technol.*, vol. 31, Jan. 2018, Art no. 025007.

[10] N. Amemiya, Y. Sogabe, S. Yamano, and H. Sakamoto, "Shielding current in a copper-plated multifilament coated conductor wound into a single pancake coil and exposed to a normal magnetic field," *Supercond. Sci. Technol.*, vol. 32, Oct. 2019, Art no. 115008.

[11] F. Grilli, and A. Kario, "How filaments can reduce AC losses in HTS coated conductors: a review," *Supercond. Sci. Technol.*, vol. 29, Jul. 2016, Art no. 083002.

[12] E. Pardo, M. Kapolka, J. Kováč, J. Šouc, F. Grilli, and A. Piqué, "Three-dimensional modeling and measurement of coupling AC loss in soldered tapes and striated coated conductors," *IEEE Trans. Appl. Supercond.*, vol. 26, no. 3, Apr. 2016, Art. no. 4700607.

[13] F. Gömöry, and J. Šouc, "Stability of DC transport in HTS conductor with local critical current reduction," *Supercond. Sci. Technol.*, vol. 34, Jan. 2021, Art no. 025005.

[14] H. Mochida, Y. Suetomi, T. Takao, H. Maeda and Y. Yanagisawa, "Continuous Heating Criteria to Avoid Thermal Runaway of Insulated HTS Coils in High Fields," *IEEE Trans. Appl. Supercond.*, vol. 29, no. 5, Aug. 2019, Art no. 4301306.

[15] L. Ren, G. Chen, Y. Xu, D. Pu, J. Xu, S. Yan, J. Shi, and L. Chen, "Experimental analysis of quench characteristic in HTS tapes and coils," *IEEE Trans. Appl. Supercond.*, vol. 29, no. 5, Aug. 2019, Art no. 4700606.

[16] H. Miyazaki, S. Iwai, T. Tosaka, K. Tasaki, S. Hanai, M. Urata, S. Ioka, and Y. Ishii, "Thermal stability of conduction-cooled YBCO pancake coil," *IEEE Trans. Appl. Supercond.*, vol. 21, no. 3, pp. 2453–2457, Jun. 2011.

[17] Y. Yanagisawa, T. Fukuda, K. Sato, H. Nakagome, T. Takao, H. Kamibayashi, M. Takahashi, and H. Maeda, "Use of a thermal grid to increase thermal runaway current for REBCO pancake coils operated at 77 K," *IEEE Trans. Appl. Supercond.*, vol. 23, no. 3, Jun. 2013, Art. no. 4603505.

[18] Y. Yanagisawa, E. Okuyama, H. Nakagome, T. Takematsu, T. Takao, M. Hamada, S. Matsumoto, T. Kiyoshi, A. Takizawa, M. Takahashi, and H. Maeda, "The mechanism of thermal runaway due to continuous local disturbances in the YBCO-coated conductor coil winding," *Supercond. Sci. Technol.*, vol. 25, Jun. 2012, Art no. 075014

[19] S. Takayama, K. Koyanagi, T. Tosaka, K. Tasaki, T. Kurusu, Y. Ishii, N. Amemiya, K. Suzuki, T. Ogitsu, Y. Iwata, and K. Noda, "Thermal Stability of Conduction-Cooled HTS Magnets for Rotating Gantry," *IEEE Trans. Appl. Supercond*., vol. 26, no. 4, Jun. 2016, Art no. 4402404.

[20] A. Badel, B. Rozier, K. Takahashi and S. Awaji, "Simulation of Local Dissipation Phenomena in the REBCO Insert of the 25-T CSM Magnet: Understanding and Preventing Destructive Thermal Runaway," *IEEE Trans. Appl. Supercond*., vol. 29, no. 5, Aug. 2019, Art no. 4600605.

[21] J. Ruuskanen, A. Stenvall, V. Lahtinen, J. van Nugteren, G. Kirby and J. Murtomäki, "How to Computationally Determine the Maximum Stable Operation Current of an HTS Magnet," *IEEE Trans. Appl. Supercond.*, vol. 29, no. 5, Aug. 2019, Art no. 4701204.

[22] A. Badel, B. Rozier, B. Ramdane, G. Meunier, and P. Tixador, "Modeling of 'quench' or the occurrence and propagation of dissipative zones in REBCO high temperature superconducting coils," *Supercond. Sci. Technol.*, vol. 32, Jul. 2019, Art. no. 094001.

[23] M. A. Green, "Quench protection solutions for magnets fabricated with insulated HTS tape conductors," *IEEE Trans. Appl. Supercond.*, vol. 28, no. 3, April 2018, Art no. 4700705.

[24] R. Matsuo, N. Matsuda, Y. Fuchida, A. Kojima, A. Nomoto, T. Takao, K. Nakamura, and O. Tsukamoto., "Study on hot-spot temperature limits of epoxy-impregnated coil wound with Bi/Ag sheathed wire to be safe from damage caused by quenches," *IEEE Trans. Appl. Supercond.*, vol. 28, no. 4, June 2018, Art no. 4703605.

[25] X. Luo, S. Inoue, N. Amemiya, "Experimental study on quench detection and protection conditions of copper-stabilized coated conductors using short samples," *IEEE Trans. Appl. Supercond.*, vol. 29, no. 8, Dec. 2019, Art. no. 4703511.

[26] H. Toriyama, A. Nomoto, T. Ichikawa, T. Takao, K. Nakamura, O. Tsukamoto, and M. Furuse, Quench protection system for an HTS coil that uses Cu tape co-wound with an HTS tape," *Supercond. Sci. Technol.*, vol. 32, Oct. 2019, Art. no. 115016.

[27] M. N. Wilson, "Protection by an external resistor," in *Superconducting Magnets*, Oxford, U.K.: Clarendon, 1983, pp. 219–221.

[28] T. Minagawa, Y. Fujimoto, and O. Tsukamoto, "Study on protection of HTS coil against quench due to temperature rise of long part of HTS

wires," *IEEE Trans. Appl. Supercond.*, vol. 23, no. 3, Jun. 2013, Art no. 4702004.

[29] G. Celentano *et al*., "Quench behavior of a conduction cooled $YBa_2Cu_3O_{7-x}$ tape pancake coil," *IEEE Trans. Appl. Supercond.*, vol. 23, no. 3, Jun. 2013, Art no. 4600704.

[30] A. Ishiyama, H. Ueda, Y. Aoki, K. Shikimachi, N. Hirano, and S. Nagaya, "Quench behavior and protection in cryocooler-cooled YBCO pancake coil for SMES," *IEEE Trans. Appl. Supercond.*, vol. 21, no. 3, pp. 2398–2401, Jun. 2011.

[31] H. Ueda, A. Ishiyama, K. Muromachi, T. Suzuki, K. Shikimachi, N. Hirano, and S. Nagaya, "Quench detection and protection of cryocooler-cooled YBCO pancake coil for SMES," *IEEE Trans. Appl. Supercond.*, vol. 22, no. 3, Jun. 2012, Art no. 4702804.

[32] Y. Iwasa, H. Lee, J. R. Fang, and B. Haid, "Quench and recovery of YBCO tape experimental and simulation results," *IEEE Trans. Appl. Supercond.*, vol. 13, no. 2, pp. 1772–1775, Jun. 2003.

[33] G. Manfreda, "Review of ROXIE's material properties database for quench simulation" CERN Internal Note 2011-24, EDMS Nr: 1178007.